



Synthesis, Characterization, Anti-corrosive/Anti-tumor Applications of a New Type Arylazo Compound 1,7-Bis(2-Hydroxy Phenyl)-4-(Phenyl Hydrazono)-Hepta-1,6-Diene-3,5-Dione

Raina Jose Cherappanath¹ · V. D. John¹

Received: 1 July 2018 / Revised: 1 September 2018 / Accepted: 4 September 2018 / Published online: 10 September 2018
© Springer Nature Switzerland AG 2018

Abstract

The purpose of the study is to synthesize and characterize a new arylazo compound 1,7-bis(2-hydroxyphenyl)-4-(phenylhydrazono)hepta-1,6-diene-3,5-dione (HPHDD). The corrosion inhibition behavior of the compound on mild steel in 1 M HCl was investigated using weight loss method, electrochemical impedance spectroscopy, and potentiodynamic measurements. The results revealed that this arylazo compound effectively inhibited the corrosion reaction in HCl medium. The surface analysis indicated that this inhibitor was strongly adsorbed on the metal surface. The electrochemical studies at different temperatures showed the thermal stability of the inhibitor. Quantum chemical studies were performed using DFT at the B3LYP/6-31G (d, p) basis set. Contrary to the carcinogenic property of usual anti-corrosive substances, the in vitro cytotoxic studies of the newly synthesized arylazo derivative against Dalton lymphoma ascites cells confirm the anti-tumor properties of the compound.

Keywords Corrosion inhibitors · Mild steel · Polarization · SEM · In vitro cytotoxic studies

1 Introduction

Corrosion which deteriorates the oil or gas pipelines or oil tanks affects the national economy and also has severe adverse effects on the ecosystem. One of the methods of combating corrosion is the use of effective non-toxic corrosion inhibitors [1, 2]. The use of corrosion inhibitors is a vital method of prevention of corrosion particularly in hydrochloric acid and sulfuric acid mediums, which are used for the pickling of aluminum and electrochemical etching. The major industries where corrosion inhibitors are used are petroleum refining, oil and gas exploration, chemical production, and water treatment plants. Anti-corrosive agents are also used in the sterilization of medical endoscopes. Many organic compounds are widely studied as corrosion inhibitors against mild steel (MS) corrosion in acid medium [3, 4]. The high inhibition efficiency of organic molecules is strictly related with its molecular structure, presence of

electronegative atoms (such as N, S, and O), unsaturated bonds, electronic properties as well as corrosive environment [5–12]. Corrosion control could be enhanced with more efficient corrosion inhibitors containing more heteroatoms. Recent studies have shown that the anti-corrosive agents used in the industry are highly toxic and carcinogenic [13, 14]. In these circumstances, there is necessity for developing effective low-cost, low-toxic, green organic corrosion inhibitor compounds.

The synthesis involves the preparation of 1,7-diaryl heptanoids using Pabon method and consequent coupling with benzene diazonium salt to form arylazo compound. The presence of electron donating centers and the C=N group in the synthesized compound prompted us to do the corrosion studies. The purpose of the present work is to investigate the corrosion inhibition efficiency of the synthesized compound for MS in IM hydrochloric acid using weight loss method, electrochemical impedance spectroscopy, and potentiodynamic measurements. The synthesized arylazo compound 1,7-bis(2-hydroxyphenyl)-4-(phenylhydrazono)hepta-1,6-diene-3,5-dione (HPHDD) molecule due to the presence of β diketo group may bind directly with DNA [15] and trigger DNA damage and also inhibit expression of DNA repair proteins in cancer cells [16] and so can be used

✉ V. D. John
rainajc@gmail.com

¹ Research and PG Department of Chemistry, Christ College, Irinjalkkuda, India

in medical field also. This instigated us to do the cytotoxic study of the newly synthesized compound.

2 Experimental Details

2.1 Materials

The MS of the following composition was used for the studies (0.2% C, 1% Mn, 0.3% P, 0.2% S, and the rest Iron). MS coupons of 1.5 cm × 1.5 cm × 1 mm were used (1 cm² exposed area). The coupons were cut and abraded with different grades of emery paper and washed with deionized water. They were then degreased with acetone to remove the possible residues of polishing and dried in air.

2.2 Test Solutions

Aggressive 1 M HCl solution was prepared by diluting analytical grade 37% HCl with deionized water. The test solutions of different concentrations of inhibitor 50 ppm, 75 ppm, 100 ppm, and 150 ppm were prepared.

2.3 Preparation of Inhibitor

2.3.1 Synthesis of 1,7-Bis(2-Hydroxyphenyl) Hepta-1,6-Diene-3,5-Dione

Acetyl acetone (0.005 mol, 0.5 g) and boric oxide (0.0035 mol, 0.25 g) were stirred about 1 h to obtain acetyl acetone–boron complex. To the reaction mixture, the salicylaldehyde (0.01 mol) dissolved in dry ethyl acetate (7.5 ml) and tri(*sec*-butyl) borate (0.02 mol, 5.4 ml) were added and the reaction mixture was stirred and the temperature was kept above 80 °C. While stirring, *n*-butyl amine (0.1 ml dissolved in 1 ml dry ethyl acetate) was added dropwise

for about 40 min. Stirring was continued for an additional period of ~4 h and the mixture was kept aside overnight. Hot (~60 °C) HCl (0.4 M, 7.5 ml) was added and then the mixture was again stirred for ~1 h. Two layers were separated and the top organic layer was extracted with 5 ml ethyl acetate. The extracts were allowed to evaporate and the residue material was stirred with concentrated HCl (10 ml) for ~1 h. The solid product separated was washed with water and dried in vacuum. A mixture of 1,7-diaryl heptanoid and 6-aryl hexanoid was obtained. The products obtained were quantitatively separated by column chromatography using silica gel (60–120 mesh) (Pabon method) [17]. The product was purified by column chromatography over silica gel (60–120 mesh) using 2:1 (v/v) chloroform:acetone mixture as the eluent and recrystallized twice from hot benzene to get pure crystalline material.

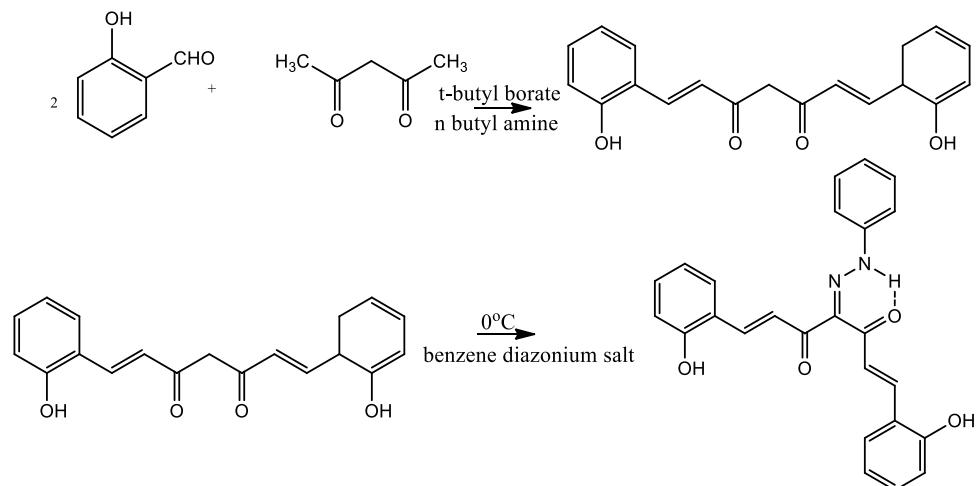
2.3.2 Synthesis of HPHDD

The arylazo derivative (HPHDD) was synthesized by the coupling of benzene diazonium salt with β-diketone [18]. Benzene diazonium salt (0.01 mol) was prepared and it was added drop by drop to a solution of the β-diketone (0.01 mol) kept below 0 °C with constant stirring. The precipitated compound was filtered, washed with water, and recrystallized from ethanol to get chromatographically pure (TLC) material; arylazo compound 91% was obtained (Scheme 1).

2.4 Weight Loss Measurements

The experiments were carried out in blank 1 M HCl and in the test solutions containing inhibitor concentrations ranging from 50 ppm to 150 ppm. The pre-weighed MS coupons were suspended in different concentrations of inhibitor in 1 M HCl solution at 28 °C using glass hooks in the absence and presence of inhibitor in aerated condition. Test coupons

Scheme 1 Synthetic route of the studied arylazo compound



were taken out and reweighed after 24 h. The difference between the initial and final weights of the coupons gave the weight loss.

2.5 Electrochemical Measurements

Electrochemical measurements were realized using computer-controlled Metrohm Autolab PGSTAT 50519. The EIS measurements were carried out using a classical three-electrode corrosion cell. A three-electrode system was used to determine the potential across electrochemical interface accurately. Saturated calomel electrode was used as the reference electrode, MS coupons with exposed surface area 1 cm² were used as the working electrode, and the Platinum electrode was used as the counter electrode. 50 ml of 1 M HCl solutions with and without inhibitor was used for the studies. After keeping the solutions for 1 h for stabilizing OCP, the values were measured. Nova Software was used to collect the experimental data. The electrochemical impedance measurements were carried out in frequency ranging from 100,000 Hz to 10⁻¹ Hz with an amplitude of 10 mV at the open circuit potential by applying AC signal. To investigate the anti-corrosive behavior of the HPHDD at different temperatures, the impedance study of the test solutions was carried out at different temperatures also. The temperature was controlled by an aqueous thermostat. The potentiodynamic measurements were carried out for cathodic and anodic part with a scan rate of 1 mV/s.

2.6 Surface Analysis

Scanning electron microscopic (SEM) analysis was carried out on SEM Jeol JSM-4500 instrument. Micrographs of the MS surface before and after 3 days immersion in 1 M HCl with and without corrosion inhibitor were taken. The energy of the acceleration beam was 20 kV and the given results are of 1000× magnitudes. EDX spectra were taken using BRUKER XFlash 6/10 instrument. The energy of the beam used was 30 MeV. AFM analysis was done using Bruker dimension edge model instrument in non-contact mode.

2.7 Quantum Chemical Studies

Quantum mechanical calculations were done on the inhibitor molecule by DFT method using B3LYP/6-31G (d, p) basis set. The structure of the inhibitor molecule for the optimization process was drawn using Gauss view 5.0. According to Koopmans' theorem, the energy of highest occupied molecular orbital (E_{HOMO}) and the energy of the lowest unoccupied molecular orbital (E_{LUMO}) of the molecule are related to ionization potential (I) and the electron

affinity (A) by the relations, $I = -E_{HOMO}$ and $A = -E_{LUMO}$. Several other Quantum chemical descriptors are to be considered in order to correlate the predicted inhibition efficiency with the experimentally determined. Absolute electronegativity (χ) is the measure of power of the atom to attract the electrons towards it. Absolute hardness (η) is the measure of resistance of an atom to charge transfer. Stability of the molecule is given by (σ). Electrophilicity index (ω) and the change in the number of electrons transferred (ΔN) can be calculated from I and A values. All the above parameters can be calculated using the following equations:

$$\chi = \frac{(I + A)}{2} \quad (1)$$

$$\eta = \frac{(I - A)}{2} \quad (2)$$

$$\sigma = \frac{1}{\eta} \quad (3)$$

$$\omega = \frac{\chi^2}{2\eta} \quad (4)$$

$$\Delta N = \frac{\chi_{Fe} - \chi_{inh}}{2(\eta_{Fe} - \eta_{inh})}, \quad (5)$$

where χ_{Fe} and χ_{inh} denote the absolute electronegativity of iron and inhibitor molecule. The η_{Fe} and η_{inh} represent absolute hardness of iron and the inhibitor molecule. The values of χ_{Fe} and χ_{inh} are taken as 7 eV mol⁻¹ and 0 eV mol⁻¹, respectively, by assuming that for a metallic bulk $I = A$.

2.8 In vitro Cytotoxicity Studies

In vitro cytotoxicity studies were carried out using the arylazo compound dissolved in minimum quantity of DMSO at Amala Cancer Research Centre, Thrissur, Kerala. The Dalton lymphoma ascites (DLA) tumor cells were aspirated from the peritoneal cavity of tumor-bearing mice. The cells were washed with phosphate-buffered saline (PBS) and centrifuged for 15 min at 1500 rpm. Viability of the cells was determined by trypan blue exclusion method [19]. Viable cells (1×10^6 cells on 0.1 ml) were added to tubes containing various concentrations of the inhibitor compound and the volume was made up to 1 ml using PBS. Control tube contains only cell suspension. Then these mixtures were incubated for 3 h at 37 °C. Further, cell suspension was mixed with 0.1 mol of 1% trypan blue and kept for 2–3 min and loaded on a hemocytometer. The number of stained (dead)

and unstained (live) cells were counted and percentage cytotoxicity was evaluated.

3 Results and Discussions

3.1 Structural Characterization

Structural characterization of the inhibitor molecule was done using C, H, N elemental analysis IR and mass spectra. The structure of the compound is shown in Fig. 1.

3.1.1 FTIR Spectrum

The IR spectrum (Fig. 2) of the synthesized compound showed the following absorption bands at 1590 cm^{-1} (C=N), 1708 cm^{-1} (free C=O). The bands are listed in Table 1.

3.1.2 ^1H NMR Spectrum

^1H NMR (CDCl_3) showed different bands at $\delta = 9.953\text{ ppm}$ (s, 1H, phenolic); $\delta = 8.671\text{ ppm}$ (s, 1H, NH) [20];

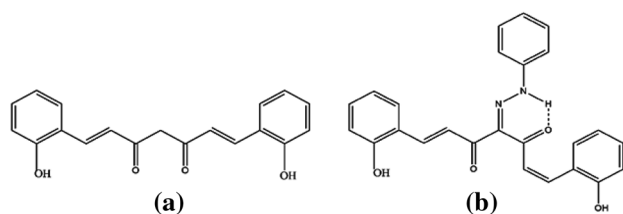


Fig. 1 The molecular structure of **a** 1,7-bis(2-hydroxyphenyl)hepta-1,6-diene-3,5-dione and **b** the inhibitor HPHDD

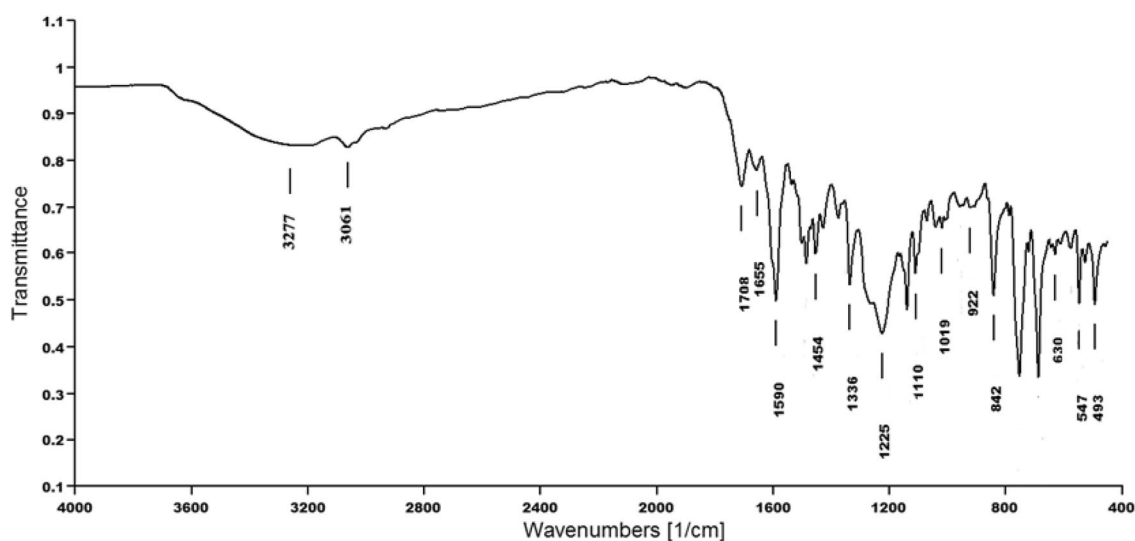


Fig. 2 IR spectrum of the synthesized inhibitor

Table 1 IR bands of synthesized arylazo compound

Assignment	Wave number (cm^{-1})
(C=N)	1590
Chelated (C=O)	1655
Free (C=O)	1708
Hydrogen bonded OH group	3277

$\delta = 7.359\text{--}7.465$ (m, aryl protons); and $\delta = 6.853\text{--}7.801$ (d, alkenyl protons). The ^1H NMR data confirmed the expected hydrogen proton distribution in the synthesized arylazo compound.

3.1.3 Mass Spectrum

The mass spectrum (Fig. 3) of the synthesized inhibitor illustrated a (M + 1) peak at m/z 413(4%) and base peak at 69 (100% $[\text{NH}=\text{N}-\text{C}=\text{C}=\text{O}]^+$) together with other significant peaks. The mass spectrum confirmed the structure of the inhibitor molecule.

3.1.4 C, H, and N Elemental Analysis

C, H, and N elemental analysis shows that the theoretical and experimental data are close approximately. This indicates the purity of synthesized inhibitor. The results obtained C (71.98%), H (4.4%), N (6.6%) are summarized in Table 2.

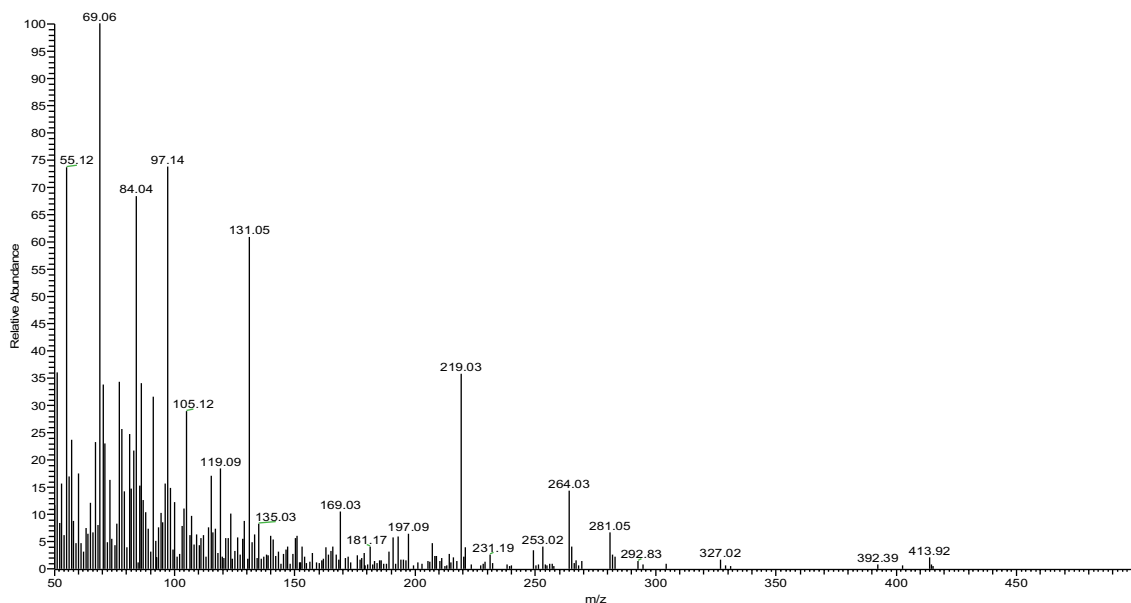


Fig. 3 Mass spectra of the inhibitor molecule

Table 2 C, H, N elemental analysis of the synthesized arylazo compound

Element %	C %	H %	N %
Found	71.98	4.4	6.6
Calculated	72.00	4.8	6.7

Table 3 Weight loss data for MS in 1 M HCl without and with different concentrations of HPHDD at 28 °C

Conc.	Arylazo (K)	η_w %	Diketone (K)	η_w %
Blank	4.401			
50 ppm	1.197	72.8	2.11	52.06
75 ppm	0.825	81.25	1.83	58.41
100 ppm	0.599	86.38	1.45	67.05
150 ppm	0.483	89.03	0.972	77.91

3.2 Weight Loss Measurements

The values of corrosion rate, inhibition efficiency (η_w), and the degree of surface coverage (θ) for MS immersed in 1 M HCl in the absence and presence of different concentrations of HPHDD from the weight loss method are shown in Table 3. The results show that the corrosion rate (k) decreases in the presence of inhibitor and the percentage of inhibition increases with increasing concentration of the inhibitor, which is due to the increased adsorption of the HPHDD on the metal surface. The corrosion rate (k) in $\text{mg cm}^{-2} \text{h}^{-1}$ was calculated by the following equation [7, 21]:

$$k = \frac{\Delta W}{S \times t} \tag{6}$$

where ΔW is the weight loss of coupon (mg), S is the total area of the coupon (cm^2), and t is the time of treatment (h). The degree of surface coverage (θ) and the inhibition efficiency η_w [22–24] were calculated using Eqs. 7, 8, respectively.

$$\theta = \frac{K_o - K}{K_o} \tag{7}$$

$$\eta_w = \frac{K_o - K}{K_o} \times 100 \tag{8}$$

where K_o and K are the values of the corrosion rate without and with inhibitor, respectively. From the results (Table 3) it is clear that inhibition efficiency increases with increase in the concentration of the inhibitor. The maximum inhibition efficiency indicates that the inhibitor adsorbed effectively on MS surface and led to the formation of a strong metal–inhibitor interaction and also it decreases the chloride ion attack on MS surface.

3.3 Comparison of Inhibition Efficiency of Arylazo Compound with Parent Diketone

The inhibition efficiencies of arylazo compound and parent diketone compound were compared using weight loss measurements of MS specimens in 1 M HCl at 28 °C. The analysis (Table 3) revealed that the inhibition efficiency of the arylazo compound is greater than the parent compound. The presence of the (C=N) group enhanced the corrosion

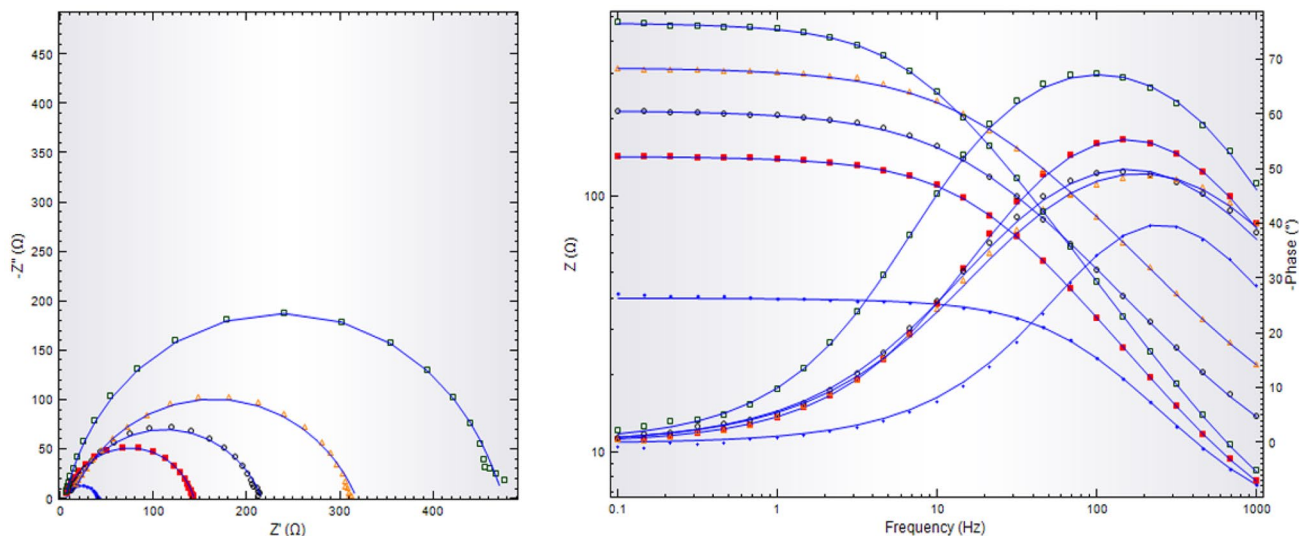


Fig. 4 EIS results of MS in 1 M HCl solution (blue-filled circle) and containing 50 ppm (red-filled square), 75 ppm (open circle), 100 ppm (yellow-filled triangle), 150 ppm (open square) of the inhibitor and the Bode plots. (Color figure online)

Table 4 The parameters obtained from fitting the EIS data in 1 M HCl test solution, for the absence and presence of inhibitor

Conc.	R_{ct} ($\Omega \text{ cm}^2$)	CPE ($\mu\text{S cm}^{-2}$)	$\eta\%$
Blank	34.9	164	
50 ppm	139	150	74.89
75 ppm	209	143	83.3
100 ppm	308	96.3	88.67
150 ppm	438	32.6	92.03

inhibition behavior of the arylazo compound. The more number of heteroatoms (electron donating centers) in the arylazo compound helps the compound to actively participate in corrosion inhibition mechanism.

3.4 Electrochemical Measurements

3.4.1 Electrochemical Impedance Spectroscopic Measurements

The behavior of the metal/solution interface was studied using electrochemical impedance spectroscopic technique. The plot of the real part of impedance against the imaginary part gives a Nyquist plot. The Nyquist plots of MS in 1 M HCl solution in the absence and presence of different concentrations of HPHDD are shown in Fig. 4. In the Nyquist plots, a depressed single capacitive loop was obtained in each case, i.e., the center of the each semicircle is depressed by an angle of $(1 - n) = 90^\circ$. The parameters associated with impedance analysis and the percentage efficiency calculated are given in Table 4.

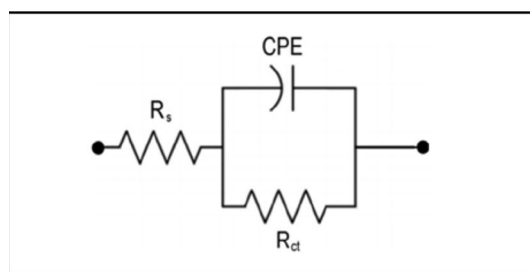


Fig. 5 Circuit diagram for EIS measurements (Randles circuit)

Electrochemical equivalent circuit model for the corrosion studies is shown in Fig. 5. The Randles circuit is one of the simplest cell models. It is used to model corrosion processes. The R_{ct} is the charge transfer resistance and R_s is the solution resistance [25]. Modeling an electrochemical phenomenon with an ideal capacitor assumes that the surface under investigation is homogenous which normally not the case is. Since the interface is not ideal, a constant phase element is used instead of pure capacitance. CPE is the constant Phase element. This non-ideal behavior can be explained with the electrical double layer theory. There exists two capacitors in serial, one between the metal and outer Helm Holtz plane and another through the Gouy Chapman diffuse layer, and as a consequence a differential capacitance behavior occurs [26]. The impedance of the CPE could be expressed as follows [27, 28]:

$$z_{CPE} = [Y_o(j\omega)^n]^{-1}, \tag{9}$$

where Y_o is the admittance of an ideal capacitance; $j^2 = -1$ is the imaginary number; ω is the angular frequency; and n

is an empirical constant ranging from 0 to 1. The n values are connected to the deviation of ideal capacitance behavior. For ideal electrodes, the value of n is equal to one and for a pure resistor n is equal to zero. The inhibition efficiency was calculated using the following equation [29, 30]:

$$\eta\% = \frac{R'_{ct} - R_{ct}}{R'_{ct}} \times 100 \quad (10)$$

where R_{ct} and R'_{ct} are the charge transfer resistances obtained in the solutions without and with inhibitor, respectively. It is evident that the R_{ct} values are increasing with increase in the concentration of the inhibitor. In case of uninhibited solution, the R_{ct} obtained was only $34.9 \Omega \text{ cm}^2$, whereas in the case of inhibitor solution, the R_{ct} obtained ($139 \Omega \text{ cm}^2$) was relatively larger when compared to the blank solution. This shows that the inhibitor molecule adsorbed on the MS surface decreases the area available for H^+ ion reduction. At the same time, the value of CPE decreases with the concentration of inhibitor as the inhibitor displaces the other ions originally adsorbed on the surface. The results show that the protective adsorption layer formed by the inhibitor molecules on metal surface provides an effective barrier to the corrosion media. The formation of a surface film by HPHDD on the MS either decreases the local dielectric constant and/or increases the thickness of electrical double layer. The $\eta\%$ value is maximum (92%) for 150 ppm of the inhibitor. The results of EIS studies are in accordance with the results obtained from weight loss method. The absolute value of impedance and phase shifts are plotted as a function of frequency in two different plots giving a Bode plot as shown in Fig. 4. This is the more complete way of presenting the data. The Bode plots show that the break point frequency shifted gradually to lower values as the concentration of the inhibitor increases. The Bode plots show a slightly broadened maximum which may account for the formation of a protective layer after 1 h of immersion time.

3.4.2 Polarization Measurements

The potentiodynamic polarization curves of the MS in 1 M HCl and at different concentrations of HPHDD are shown in Fig. 6. Using the Nova Software, the cathodic and anodic slopes of Tafel plots were determined. The corresponding corrosion potential (E_{corr}) and current density (I_{corr}) obtained are given in Table 5. The Tafel plots show that the addition of HPHDD has a pronounced inhibitive effect on the anodic and cathodic part of the curves, while the corrosion potential (E_{corr}) is only slightly shifted. In the inhibited solution, the E_{corr} has shifted to more negative direction than the uninhibited solution. This negative shift of E_{corr} indicates that this Schiff base has the ability

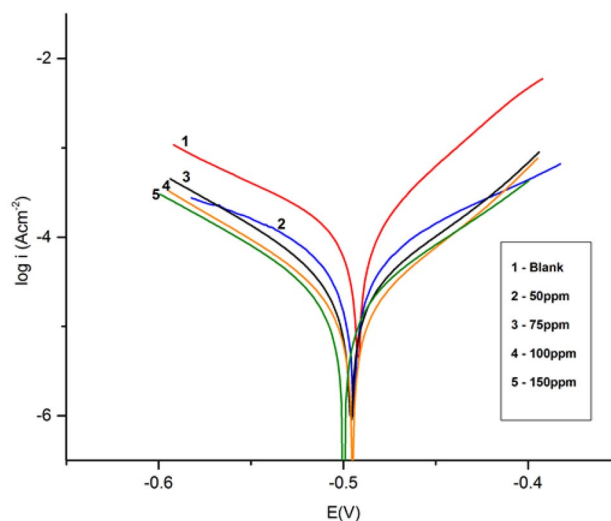


Fig. 6 Potentiodynamic polarization curves for mild steel in 1 M HCl solution at different concentrations of the inhibitor

to inhibit the acid corrosion of MS. The literature suggests that if the corrosion potential displacement on addition of inhibitor is greater than 85 mV, the inhibitor can be classified as cathodic or anodic type and if it is less than 85 mV, then the inhibitor can be considered as a mixed type of inhibitor [31]. Hence HPHDD can be considered as a mixed type inhibitor.

The polarization curves show that the cathodic and anodic current densities are decreasing gradually with increasing concentrations of the inhibitor. The values of the slopes β_a and β_b of the Tafel plots are decreasing which confirms that the inhibitor is not influencing the corrosion reactions; instead HPHDD is forming a barrier film on metal surface creating a substantial resistance against the charge transfer at the interface [32]. A more pronounced decrease in cathodic part indicates that the inhibitor affects the cathodic branch of corrosion process in a significant manner. This is due to a greater suppression of the cathodic hydrogen evolution than the anodic metal dissolution. The results (Table 5) indicate a significant lowering in the values of I_{corr} with the increasing concentration of HPHDD. The inhibition efficiencies were calculated from polarization measurements according to the relation [33].

$$\eta\% = \frac{I_{\text{corr}}^* - I_{\text{corr}}}{I_{\text{corr}}^*} \times 100 \quad (11)$$

where I_{corr}^* and I_{corr} are the corrosion current densities without and with inhibitor, respectively. The results show that the inhibition efficiency increased considerably with increase in the concentration of inhibitor, reaching a maximum of 93.98% for 150 ppm of inhibitor. The potentiodynamic

measurements reveal that HPHDD is a good corrosion inhibitor for MS against 1 M HCl solution.

3.4.3 Effect of Temperature

The EIS measurements were also realized in temperature range from 28 to 50 °C to study the thermal stability of the inhibitor molecule. The EIS results obtained for 1 M HCl solution in the absence and presence of 100 ppm of inhibitor at different temperatures were studied (Figs. 7, 8). The charge transfer resistance, CPE, and efficiency calculated are listed in Table 6. The R_{ct} values decreased and CPE values increased gradually with temperature. At 50 °C, the R_{ct} values of blank and 100 ppm of inhibitor are 22.5 Ω cm² and 106 Ω cm² respectively. At 50 °C, an efficiency of 78% is observed. The decrease may be due to the desorption of the inhibitor molecules from the adsorption sites at high temperature.

3.5 Adsorption Isotherms

Adsorption isotherms provide information about the mechanism of adsorption and surface behavior of adsorbed species.

Attempts were made to fit the data from polarization curves to most common adsorption isotherms. The Langmuir isotherm (Fig. 9) was found to fit best for HPHDD which confirms the adsorption of inhibitor molecules on the metal surface. The Langmuir isotherm for monolayer adsorption can be formulated as

$$\frac{C_{inh}}{\theta} = \frac{1}{K_{ads}} + C_{inh}, \tag{12}$$

where C_{inh} is the concentration of the inhibitor; θ is the fractional surface coverage; and K is the adsorption equilibrium constant. The intercept of the plot gives the value of K_{ads} . This value was calculated as $1.5321 \times 10^4 \text{ M}^{-1}$, which indicates that a high proportion of HPHDD is adsorbed on steel surface [34, 35]. The K_{ads} and ΔG° are related by the equation

$$\Delta G^\circ = -RT \ln (55.5 K_{ads}), \tag{13}$$

where R is the universal gas constant and T is the temperature in kelvin.

The calculated value of ΔG°_{ads} is -34.17 kJ/mol . The negative values of ΔG°_{ads} indicate that the adsorption of

Table 5 Electrochemical parameters for MS in 1 M HCl solution containing different concentrations of the inhibitor

Conc. (ppm)	β_a (mV/dec)	$-\beta_c$ (mV/dec)	E_{corr} vs. SCE (V)	j_{corr} ($\mu\text{A}/\text{cm}^2$)	θ	$\eta\%$
Blank	75	112	-0.493	209.95		
50 ppm	76	92	-0.494	38.947	0.8145	81.45
75 ppm	74	88	-0.496	34.236	0.8369	83.69
100 ppm	68	82	-0.495	20.318	0.9032	90.32
150 ppm	72	87	-0.499	12.629	0.9398	93.98

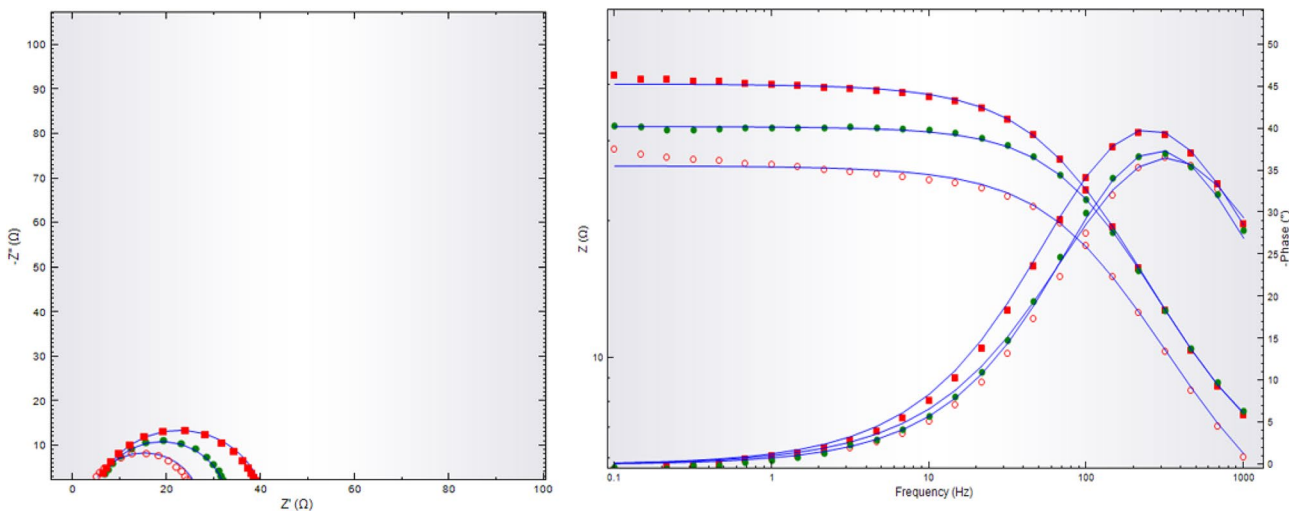


Fig. 7 EIS results of MS in 1 M HCl at different temperatures (red-filled square) 28 °C, (green-filled circle) 40 °C, (red open circle) 50 °C. (Color figure online)

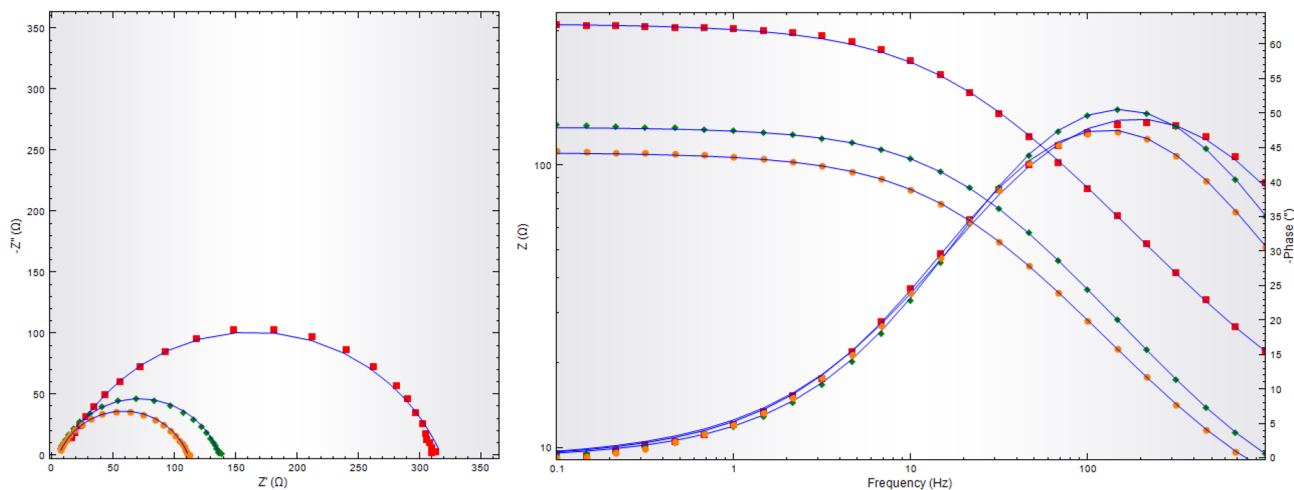


Fig. 8 EIS results of MS in 100 ppm of the inhibitor at different temperatures (red-filled square) 28 °C, (green-filled diamond) 40 °C, (yellow-filled circle) 50 °C. (Color figure online)

Table 6 The parameters obtained from fitting the EIS data in 1 M HCl test solution and in the presence of 100 ppm of inhibitor at different temperatures

Temperature (°C)	R_{ct} ($\Omega\text{ cm}^2$) Blank	CPE ($\mu\text{S cm}^{-2}$) Blank	R_{ct} ($\Omega\text{ cm}^2$) Inhibitor	CPE ($\mu\text{S cm}^{-2}$) Inhibitor	$\eta\%$
28	34.9	164	308	96.3	88.67
40	26.8	179	131	168	84.05
50	22.5	226	106	253	78.77

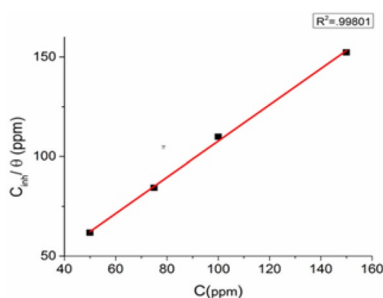


Fig. 9 Langmuir adsorption isotherm for MS in 1 M HCl solution containing different concentrations of the inhibitor

HPHDD on the metal surface is a spontaneous process. The studies reveal that the value of ΔG_{ads}° up to -20 kJ/mol or lower is consistent with electrostatic interactions between the charged inhibitor molecule and charged metal which indicates a process of physisorption. The ΔG_{ads}° value around -40 kJ/mol or higher is considered as evidence for coordinate covalent bonding of molecules on metal surface (chemisorption) [36, 37]. The obtained ΔG_{ads}° value -34.17 kJ/mol suggests that the HPHDD adsorption on MS is not merely physisorption or chemisorption but includes a comprehensive adsorption of both.

3.6 Surface Analysis

SEM images recorded were used to study the surface morphology of MS specimen in acidic solution. Figure 10a–c shows the 1000 times magnified images of polished MS, the corroded MS in HCl solution, and the surface of MS immersed in 1 M HCl solution containing 150 ppm inhibitor for 3 days, respectively. A number of pits and cracks are seen in the SEM image of MS immersed in HCl solution (Fig. 10b). These are the results of aggressive action of HCl on MS Surface. In the presence of inhibitor (Fig. 10c), the surface is free from the pits and cracks except polishing line. This is due to the formation of a barrier film by the inhibitor. The inhibitor prevents the metal dissolution and protects the MS from corrosion. The protective film formed may be decreasing the surface area available for the reduction of H^+ ions and thereby acting as a strong barrier to further anodic metal dissolution.

Energy dispersive X-ray (EDX) spectra were used to determine the elements present on the MS surface before and after exposure to the inhibitor solution. Figure 11 shows the EDX spectra of the MS surface in the absence and the presence of inhibitor solution. In uninhibited solution, only the peaks for iron and oxygen are present on the sample. In the spectra of the inhibited solution, there is a peak for nitrogen and a more enhanced peak for oxygen. The data

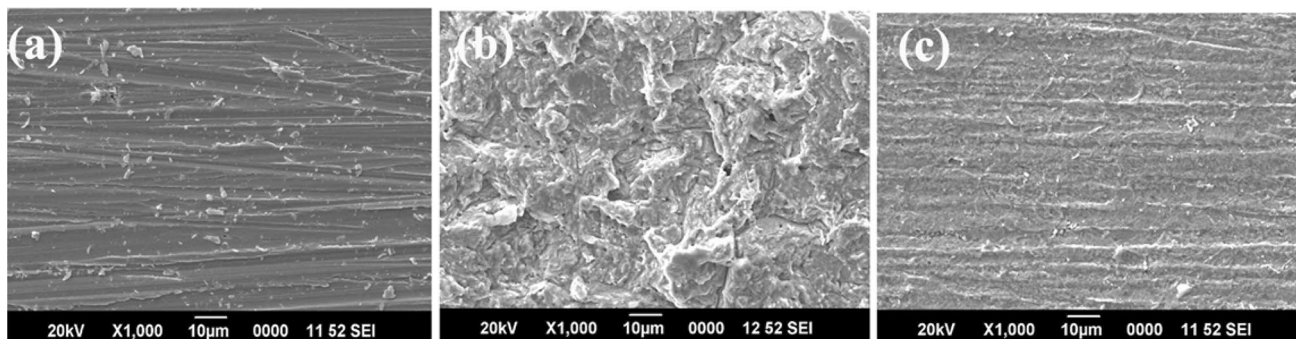


Fig. 10 SEM images of polished MS (a), MS in the absence (b) and the presence of 150 ppm of the inhibitor (c) after 3 days of immersion time

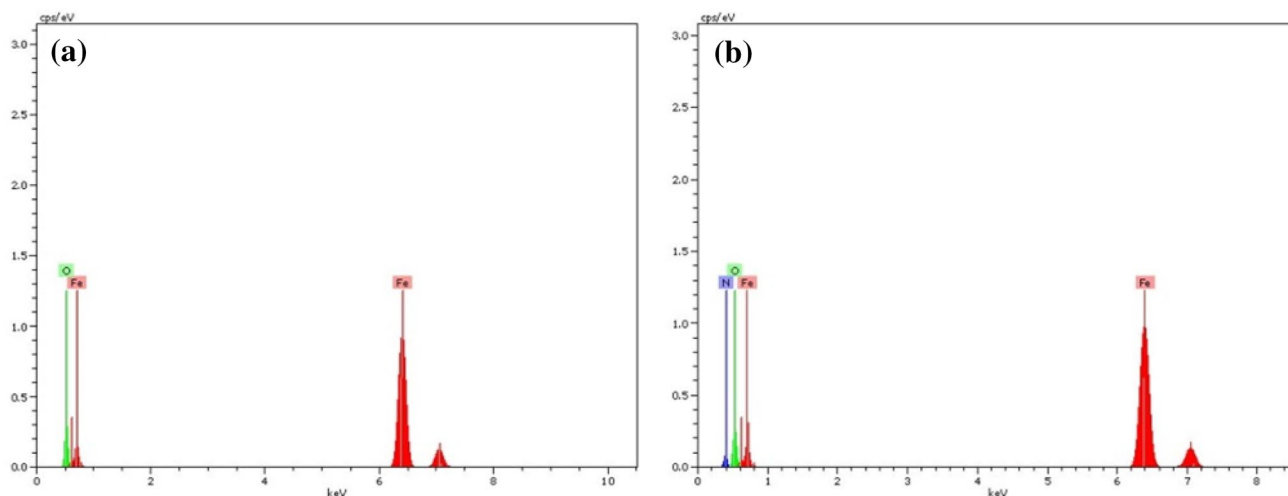


Fig. 11 EDX spectra of MS in the absence (a) and presence of 150 ppm of the inhibitor (b)

reveal the presence of an organic compound containing oxygen and nitrogen on sample surface. The higher electron density on the functional groups leads to the formation of a surface film through greater adsorption and consequently higher inhibition.

AFM is the most versatile and powerful microscopy technology for studying the surface morphology of samples at nano to microscale. The two-dimensional and three-dimensional AFM images of the MS surface exposed to 1 M HCl solution and with 100 ppm of HPHDD for 72 h are given in Fig. 12. The AFM images of MS in 1 M HCl (Fig. 12a, b) show the presence of many narrow pits of few micrometer ranges. The metal in the pit dissolves along with the reduction of oxygen. The rapid dissolution of metal in the pit results in a build-up of excessive positive charge in the pit followed by the migration of chloride ion into the pits to maintain the electroneutrality condition. Thus, high concentration of chloride ions, along

with low solution pH values, strongly favors the process of corrosion. Fig. 12c, d shows the MS surface exposed to 100 ppm of the inhibitor for 72 h which shows the presence of a uniform inhibitor layer over the MS surface due to the adsorption of the inhibitor on the MS surface. The protective barrier film formed prevents the pitting process thereby increasing the inhibition efficiency.

3.7 Quantum Chemical Studies

Quantum chemical calculations (using DFT method) were performed to investigate the effect of different physiochemical parameters such as chemical structure, charge density at the active centers (heteroatoms) of the molecule, and the mode of adsorption on the inhibition efficiency of the inhibitor. The optimized molecular structure and their calculated HOMO and LUMO levels of corrosion inhibitor HPHDD are shown in Fig. 13. Quantum chemical parameters obtained such as

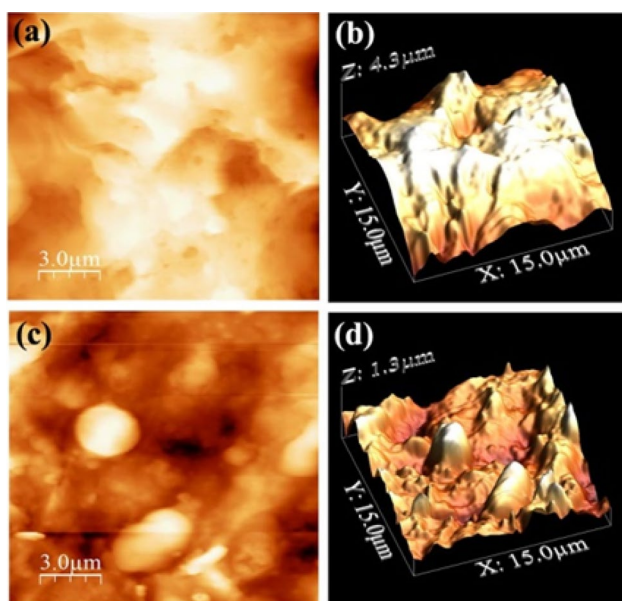


Fig. 12 AFM images of MS in the absence (a, b) and presence of 150 ppm of the inhibitor (c, d)

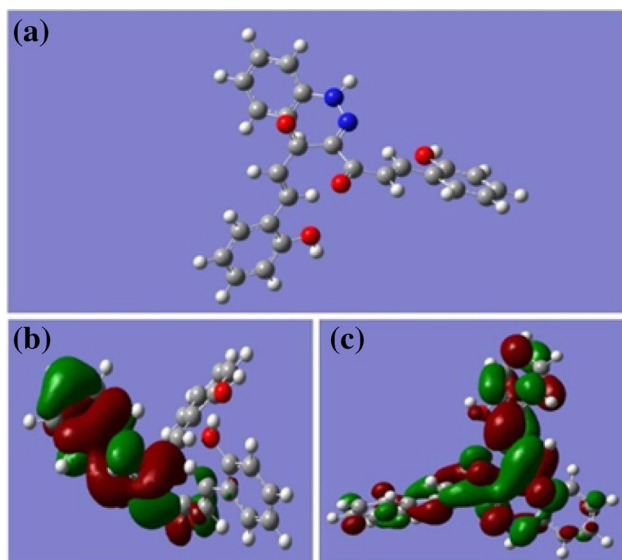


Fig. 13 The optimized molecular structure (a) and their calculated HOMO (b) and LUMO (c) levels of corrosion inhibitor HPHDD using DFT at the B3LYP/6-31G (d, p) basis set

the energy of highest occupied molecular orbital (E_{HOMO}), the energy of the lowest unoccupied molecular orbital (E_{LUMO}), and the dipole moment (μ) of the molecule obtained are given in Table 7. Different parameters are used to explain the electron transfer mechanism between inhibitor molecule and the metal surface. The ionization potential (I), the electron affinity (A), absolute electronegativity (χ), absolute hardness (η), stability of the molecule (σ), electrophilicity index (ω), and the change in the number of electrons transferred (ΔN) are the important parameters used to reveal the electron transfer mechanism between inhibitor molecule and the metal surface which are calculated and collected in Table 7. The high value of E_{HOMO} indicates the tendency to donate electrons and the lower value of E_{LUMO} shows the ability of the molecule to accept electrons. The energy values obtained suggest the better inhibition efficiency of the compound. The lower energy gap (ΔE) shows the higher reactive nature of the molecule which in turn increases the inhibition efficiency. From the earlier studies it is clear that if the ΔN value is less than 3.6 ($\Delta N < 3.6$), the inhibition efficiency of the inhibitor enhances by increasing the electron donation to the metal surface. The ΔN value obtained in the study proves that the synthesized compound is a good inhibitor. Mulliken charges on heteroatoms determined by optimization process are presented in Table 8.

The two types of adsorption responsible for the formation of protective layer are physisorption and chemisorption. The calculations show that there is more than one active center in the inhibitor molecule and all the active centers (heteroatoms) carry a high value of negative charge. These negatively charged heteroatoms can easily donate the electrons to the vacant d orbitals of the metal which results in the physisorption. Chemisorption can be better explained as the aromatic ring moiety of the inhibitor donates the π electrons and the heteroatoms donate the lone pair of electrons to the metal surface. A molecule with more planarity may be considered as a good inhibitor rather than a molecule with less planarity. The optimized structure clearly shows the planarity of the aromatic rings. This again correlates with high inhibition efficiency of the mixed type inhibitor HPHDD.

3.8 Mechanism of Inhibition

The arylazo molecule exists as protonated through nitrogen atoms in HCl solutions and the protonated inhibitor molecule

Table 7 Quantum chemical parameters for the inhibitor with the DFT at the B3LYP/6-31G (d, p) basis set

E_{HOMO}	E_{LUMO}	ΔE	I	A	μ	χ	σ	ω	ΔN
-5.684	-1.852	3.833 eV	5.684 eV	1.852 eV	7.974 D	3.768 eV	0.522	3.704	0.8433

Table 8 Calculated Mulliken atomic charges for heteroatoms of the inhibitor using DFT at the B3LYP/6-31G (d, p) basis set

Atoms	Mulliken charges
15 O	-0.4959
18 N	-0.2933
19 N	-0.4238
33 O	-0.4719
37 O	-0.5578
50 O	-0.5572

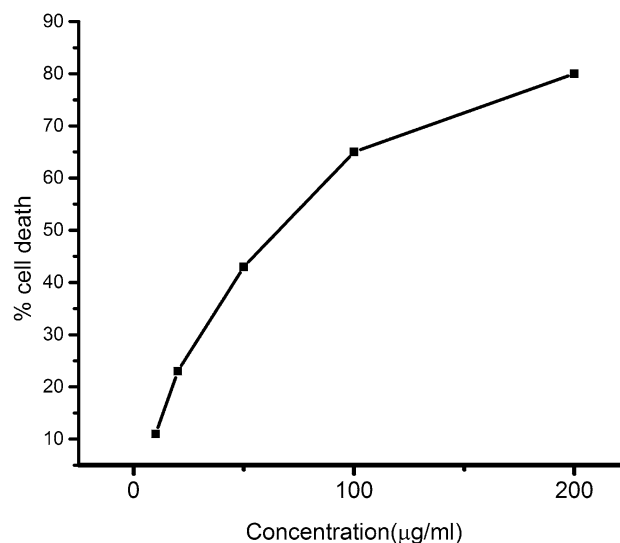
could be assorted on the metal surface via chloride ions. This will cause an electrostatic attraction between the protonated inhibitor molecules and the metal surface. After the first electrostatic adsorption of the inhibitor molecules, via, formerly adsorbed chloride ions, the inhibitor molecule would directly be adsorbed on to the metal surface. The anodic sites on metal surface have vacant d orbitals of Fe^{2+} ions, which interact with the electrons of the inhibitor and adsorb the inhibitor leading to the formation of a strong barrier film on metal surface. The presence of π electrons and the non-bonded electrons of sulfur, nitrogen, and oxygen contributes to the strong metal inhibitor interaction. Besides, the double bonds present in the inhibitor molecule allow the back donation of metal d electrons to the π^* orbital. Moreover, the adsorption of the inhibitors containing aromatic rings occurs mostly normal to the surface thereby inhibiting the corrosion by geometric blocking of the available cathodic and anodic sites on the metal surface.

3.9 In vitro Cytotoxicity

The results of in vitro cytotoxicity studies of HPHDD towards DLA cells are shown in Fig. 11. The test compound was prepared in various concentrations ranging from 10 $\mu\text{g}/\text{ml}$ to 200 $\mu\text{g}/\text{ml}$. The cytotoxicity of the compounds was determined in terms of percentage cell death produced by them. The cell death of DLA at the highest quantities of the inhibitor (200 $\mu\text{g}/\text{ml}$) was 80%. This indicates that the synthesized arylazo compound shows high degree of anti-tumor activity and is completely non-toxic and the inhibitor can be considered as an anti-tumor agent. The cytotoxic activity of the HPHDD is due to its unique structure which is similar to the 1,7-di aryl heptanoids (curcuminoids), the bioactive compounds with strong medicinal properties found in turmeric (Table 9; Fig. 14).

Table 9 In vitro cytotoxic studies of inhibitor HPHDD towards DLA

Drug con. ($\mu\text{g}/\text{ml}$)	10	20	50	100	200
% Cell death	11	23	43	65	80

**Fig. 14** The results of in vitro cytotoxicity studies of HPHDD towards DLA

4 Conclusions

The inhibition efficiency of synthesized arylazo compound HPHDD has been investigated for MS corrosion in 1 M HCl solution. The electrochemical and non-electro chemical methods were made use of for the studies. The HPHDD is found to be a good anti-corrosive agent for MS against 1 M HCl corrosion. The inhibition efficiency increased with increasing inhibitor concentration. An efficiency of 93.98% was obtained by using 150 ppm of HPHDD. The anti-corrosive activity is mainly due to the adsorption of HPHDD on the MS surface. Reasonably good agreement exists between the values obtained from weight loss method, electrochemical impedance method, and Tafel extrapolation method. The synthesized compound is found to be a mixed type inhibitor affecting both cathodic and anodic sites. The EIS studies conducted at different temperatures revealed the efficiency of HPHDD at high temperatures. The adsorption obeyed Langmuir adsorption isotherm and regarded as a combined effect of both physical and chemical adsorption. The SEM images, the EDX spectra, and the AFM analysis confirm the formation of an inhibitor layer on MS surface. From the cytotoxic studies, the synthesized arylazo compound is assigned as good anti-cancerous compound.

Acknowledgements The authors are grateful to University Grant Commission for the funding for FDP, P.G., and Research Department of Chemistry, Christ College, Irinjalakuda, Calicut University, National Institute of Technology Trivandrum, CUSAT Cochin, and Amala Cancer Research Centre, Thrissur, Kerala.

Funding Funding was provided by UGC-DAE Consortium for Scientific Research, University Grants Commission (IN) (Grant No. FIP/12 Plan/KLCA 020).

References

- Akrouf H, Maximovitch S, Bousselmi L, Triki E, Dalard F (2007) Evaluation of corrosion non toxic inhibitor adsorption for steel in near neutral solution: L (+) ascorbic acid. *Mater Corros* 58:202–206
- Akrouf H, Bousselmi L, Triki E, Maximovitch S, Dalard F (2005) Adsorption mechanism of non-toxic organic inhibitors on steel in solutions at pH 8 determined by electrochemical quartz crystal microbalance measurements. *Mater Corros* 56:185–191
- Hosseini MG, Ehteshamzadeh M, Shahrabi T (2007) Protection of mild steel corrosion with Schiff bases in 0.5 M H₂SO₄ solution. *Electrochim Acta* 52:3680–3685
- Emregül KC, Atakol O (2004) Corrosion inhibition of iron in 1 M HCl solution with Schiff base compounds and derivatives. *Mater Chem Phys* 83:373–379
- Aysel Yurt ÖA (2011) Diphenolic Schiff bases as corrosion inhibitors for aluminium in 0.1 M HCl: potentiodynamic polarisation and EQCM investigations. *Corros Sci* 53:3725–3732
- Erbil M, Tüken T, Demir F, Kıcırcı N, Sığ G (2012) Inhibition effect of 1-ethyl-3-methylimidazolium dicyanamide against steel corrosion. *Corros Sci* 59:110–118
- Soliman SA, Metwally MS, Selim SR, Bedair MA, Abbas MA (2014) Corrosion inhibition and adsorption behavior of new Schiff base surfactant on steel in acidic environment: experimental and theoretical studies. *J Ind Eng Chem* 20:4311–4320
- Arab ST, Noor EAA (1993) Inhibition of acid corrosion of steel by some S-alkylisothiuronium Iodides. *Corrosion* 49:122–129
- Elmsellem H, Harit T, Aouniti A, Malek F (2015) Adsorption properties and inhibition of mild steel corrosion in 1 M HCl solution by some bipyrazolic derivatives: experimental and theoretical investigations. *Prot Met Phys Chem Surf* 51:873–884
- Chen S, Kar T (2012) Theoretical investigation of inhibition efficiencies of some schiff bases as corrosion inhibitors of aluminum. *Int J Electrochem Sci* 7:6265–6275
- Belghiti ME et al (2016) Anti-corrosive properties of 4-amino-3,5-bis(disubstituted)-1,2,4-triazole derivatives on mild steel corrosion in 2 M H₃PO₄ solution: experimental and theoretical studies. *J Mol Liq* 216:874–886
- Agrawal YK, Talati JD, Shah MD, Desai MN, Shah NK (2004) Schiff bases of ethylenediamine as corrosion inhibitors of zinc in sulphuric acid. *Corros Sci* 46:633–651
- Oguzie EE (2005) Corrosion inhibition of mild steel in hydrochloric acid solution by methylene blue dye. *Mater Lett* 59:1076–1079
- Zucchi F, Trabaneli G, Brunoro G (1992) The influence of the chromium content on the inhibitive efficiency of some organic compounds. *Corros Sci* 33:1135–1139
- Noor Hasima, Bharat B, Aggarwal (2012) Cancer-linked targets modulated by Curcumin. *Int J Biochem Mol Biol* 3:328–351
- Mark R, Kelley D, Logden, Mellssa L, Fishell (2014) Targeting DNA repair pathways for cancer treatment: what's new. *Future Oncol* 10:1215–1237
- Krishnankutty K, John VD (2003) Synthesis, characterization, and antitumour studies of metal chelates of some synthetic curcuminoids. *Synth React Inorg Met Org Chem* 33:343–358
- Krishnankutty K, Basheer M, Kamalakshy D (2009) Arylazo derivatives of some fluorinated β -diketones and their metal complexes. *J Iran Chem Res* 2:111–119
- John VD, Ummathur MB, Krishnankutty K (2013) Synthesis, characterization, and antitumour studies of some curcuminoid analogues and their aluminum complexes. *J Coord Chem* 66:1508–1518
- Tan SF, Ang KP, How GF (1991) Intermolecular and intramolecular hydrogen bonding in 5-pyridylmethylenediamines: IR and NMR study. *J Phys Org Chem* 4, 170–176
- Li X, Deng S, Xie X (2014) Inhibition effect of tetradecylpyridinium bromide on the corrosion of cold rolled steel in 7.0 M H₃PO₄. *Arab J Chem*. <https://doi.org/10.1016/j.arabjc.2014.05.004>
- Elkacimi Y, Achnin M, Aouine Y, Touhami ME, Alami A (2012) Inhibition of mild steel corrosion by some phenyltetrazole substituted compounds in hydrochloric acid. *Port Electrochim Acta* 30:53–65
- Manjula P, Manonmani S, Jayaram P, S. R (2001) Corrosion behaviour of carbon steel in the presence of N-cetyl-N, N, N-trimethylammonium bromide, zinc and calcium gluconate. *Anti-Corros Methods Mater* 48:319–324
- Bedair MA, Soliman SA, Metwally MS (2016) Synthesis and characterization of some nonionic surfactants as corrosion inhibitors for steel in 1.0 M HCl. *J Ind Eng Chem* 41:10–22
- Singh A, Avyaya JN, Quraishi MA (2012) Schiff' s base derived from the pharmaceutical drug Dapsone (DS) as a new and effective corrosion inhibitor for mild steel in hydrochloric acid. *Res Chem Intermed*. <https://doi.org/10.1007/s11164-012-0577-y>
- Gokmen SI, Erbil M (2016) Assessment of the inhibition efficiency of 3, 4-diaminobenzonitrile against the corrosion of steel. *Corros Sci* 102, 437–445
- Manivel A, Ramkumar S, Wu JJ, Asiri AM, Anandan S (2014) Exploration of (S)-4, 5, 6, 7-tetrahydrobenzo [d] thiazole-2, 6-diamine as feasible corrosion inhibitor for mild steel in acidic media. *J Environ Chem Eng* 2:463–470
- Hassan HH (2007) Inhibition of mild steel corrosion in hydrochloric acid solution by triazole derivatives. Part II: time and temperature effects and thermodynamic treatments. *Electrochim Acta* 53:1722–1730
- Yurt A, Balaban A, Kandemir SU, Bereket G, Erk B (2004) Investigation on some Schiff bases as HCl corrosion inhibitors for carbon steel. *Mater Chem Phys* 85:420–426
- Hassan HH, Abdelghani E, Amin MA (2007) Inhibition of mild steel corrosion in hydrochloric acid solution by triazole derivatives Part I. Polarization and EIS studies. *Electrochim Acta* 52:6359–6366
- Bouanis M et al (2016) Corrosion inhibition performance of HCl solution: gravimetric, electrochemical and XPS studies. *Appl Surf Sci* 389:952–966
- Mazumder MAJ, Al-Muallem HA, Faiz M, Ali SA (2014) Design and synthesis of a novel class of inhibitors for mild steel corrosion in acidic and carbon dioxide-saturated saline media. *Corros Sci* 87:187–198
- Solmaz R, Kardas G (2008) Investigation of adsorption and inhibitive effect of 2-mercaptotiazoline on corrosion of mild steel in hydrochloric acid media. *Electrochim Acta* 53:5941–5952
- Xu B, Liu Y, Yin X, Yang W, Chen Y (2013) Experimental and theoretical study of corrosion inhibition of 3-pyridinecarboxaldehyde thiosemicarbazone for mild steel in hydrochloric acid. *Corros Sci* 74:206–213
- Zhou X, Yang H, Wang F (2011) *Electrochimica Acta* [BMIM] BF₄ ionic liquids as effective inhibitor for carbon steel in alkaline chloride solution. *Electrochim Acta* 56:4268–4275
- Likhanova NV et al (2010) The effect of ionic liquids with imidazolium and pyridinium cations on the corrosion inhibition of mild steel in acidic environment. *Corros Sci* 52:2088–2097
- El-lateef HMA (2014) Experimental and computational Investigation on the corrosion inhibition characteristics of mild steel by some novel synthesized imines in hydrochloric acid solutions. *Corros Sci*. <https://doi.org/10.1016/j.corsci.2014.11.040>